Pyk2 and bone cell anoikis with glucocorticoids

Glucocorticoid-induced bone fragility is prevented in female mice by blocking Pyk2/anoikis signaling

Amy Y. Sato,[1] Meloney Cregor,[1] Kevin McAndrews,[1] Troy Li,[1] Keith W. Condon,[1] Lilian I. Plotkin,[1] and Teresita Bellido,[1,2,3]

[1]Department of Anatomy and Cell Biology; and [2]Department of Internal Medicine, Division of Endocrinology, Indiana University School of Medicine; [3]Roudebush Veterans Administration Medical Center, Indianapolis, Indiana, USA.

ORCiD numbers:

0000-0001-5061-1369

Sato

Amy Y

0000-0002-8203-7004

Bellido

Teresita

Received 22 March 2019. Accepted 02 May 2019.

Excess of glucocorticoids (GC) is a leading cause of bone fragility, and novel therapeutic targets are sorely needed. We report that genetic deletion or pharmacological inhibition of proline-rich tyrosine kinase 2 (Pyk2) prevents GC-induced bone loss, by overriding GC effects of detachment-induced bone cell apoptosis (anoikis). In wild type (WT) or vehicle-treated mice, GC either prevented osteoclast apoptosis or promoted osteoblast/osteocyte apoptosis. In contrast, mice lacking Pyk2 (KO) or treated with Pyk2 kinase inhibitor PF-431396 (PF) were protected. KO or PF-treated mice were also protected from GC-induced bone resorption, microarchitecture deterioration, and weakening of biomechanical properties. In KO and PF-treated mice, GC increased osteoclasts in bone and circulating TRAP5b, an index of osteoclast number. However, bone surfaces covered by osteoclasts and circulating CTX, an index of osteoclast function, were not increased. The mismatch between osteoclast number vs function induced by Pyk2 deficiency/inhibition was due to osteoclast detachment and anoikis. Further, GC prolongation of osteoclast lifespan was absent in KO and PF-treated osteoclasts, demonstrating Pyk2 as an intrinsic osteoclast-survival regulator. Circumventing Pyk2 activation preserves skeletal integrity by preventing GC effects on bone cell survival (pro-apoptotic for osteoblasts/osteocytes, anti-apoptotic for osteoclasts) and GC-induced bone resorption. Thus, Pyk2/anoikis signaling as a new therapeutic target for GC-induced osteoporosis.

Introduction

Glucocorticoids (GC), produced and released by the adrenal glands, regulate numerous physiological processes in a wide range of tissues (1;2). Because of their profound immunosuppressive and anti-inflammatory actions, these agents are widely prescribed to treat an

extensive array of pathological conditions, including rheumatoid arthritis, asthma, inflammatory bowel disease, chronic lung, liver and skin diseases, as well as for the management of organ transplantation and as components of chemotherapy regimens for cancers (3). However, pharmacological administration of GC, similar to pathologic endogenous elevation, is associated with severe adverse side effects manifested in several tissues and organs, in particular the skeleton (4). Prolonged GC administration leads to a prominent loss of bone mass and strength and increased risk for atraumatic fractures in approximately 30-50% of patients (4;5). The initial rapid bone loss induced by GC is due to exaggerated bone resorption and is accompanied by suppressed bone formation. Excess GC also causes muscle weakness with the consequent loss of body balance and increased propensity to fall, which contribute to the risk of bone fractures (6-8).

The current standard of care, bisphosphonates (4), as well as the anti-RANKL antibody recently approved by the FDA to treat GC-induced osteoporosis (9), effectively prevent bone loss by inhibiting resorption. However, these agents lead to further reduction in bone formation compared to GC alone, thus preventing rebuilding the bone that was lost (10-12). In addition, profound reduction in bone turnover is not desirable since it leads to accumulation of microdamage and advanced glycation endproducts, which are associated with osteonecrosis of the jaw with long-term treatments (13;14). Severe suppression of bone turnover can also reduce toughness, the energy that bone tissue absorbs before failure, with potential increased risk of low-energy atypical fractures (13). Thus, there is an unmet need for therapeutic interventions that prevent GC-induced bone disease that lack these skeletal complications.

Deterioration of bone tissue is due to direct effects of GC on bone cells (15;16). Rapid increased bone resorption is caused by accumulation of osteoclasts on bone surfaces, resulting from stimulation of osteoclast generation combined with prolongation of the lifespan of preexisting osteoclasts (17). In addition, GC drastically inhibit bone formation, by suppressing the synthetic capacity of osteoblasts (inhibiting osteocalcin and collagen 1 synthesis and stimulating Wnt antagonist production) and by promoting osteoblast and osteocyte apoptosis (18). A remarkable feature of GC effects on bone is the opposing regulation of apoptosis depending on the bone cell lineage, i.e. anti-apoptotic for osteoclasts and pro-apoptotic for osteoblasts/osteocytes. However, the underlying mechanism of this hallmark have remained elusive.

All osteoclasts die by apoptosis upon completing resorption (19). Failure to timely undergo apoptosis is associated with increased depth of resorption pits, which leads to cortical and trabecular bone thinning, and to trabeculae perforation and loss of connectivity in cancellous bone (20). Most osteoblasts (~70% in human bone) also undergo apoptosis after producing bone matrix proteins; and osteocytes, although long-lived cells, can prematurely apoptose due to changes in hormonal as well as mechanical cues (21). The survival of bone cells is critically dependent of their attachment to the surrounding bone matrix through integrins. Signaling mediated by integrins is bidirectional. Extracellular matrix proteins bind to integrins and activate intracellular pathways, referred to as “outside-in” signaling. In turn, activation of intracellular pathways alter the interaction of integrins with the surrounding matrix, referred to as “inside-out” signaling. Disrupted interactions between integrins and the extracellular matrix leads to detachment and apoptosis (termed *anoikis*, the Greek word for homelessness) of both osteoclasts and osteoblastic cells (22;23). In particular, GC activate in cultured osteocytic cells the proline-rich tyrosine kinase 2 (Pyk2), a member of the focal adhesion kinase (FAK) family of nonreceptor tyrosine kinases, which in turn induces osteocytic cell detachment and anoikis (23).

However, whether this pathway is involved in the opposing effects of GC on osteoblast/osteocyte vs osteoclast apoptosis *in vivo* had remained unknown.

We report herein that Pyk2 is an essential mediator of anoikis regulated by GC *in vivo* in bone cells of both lineages: osteoclasts and osteocytes/osteoblasts. Pyk2 activation is required for GC-induced prolongation of osteoclast lifespan and, conversely, for promotion of osteoblast and osteocyte apoptosis. Moreover, circumventing Pyk2 activation by genetic or pharmacological means prevents GC-induced bone loss and increased skeletal fragility, by stimulating anoikis of osteoclasts while preventing anoikis of osteoblasts and osteocytes. Furthermore, overriding GC effects on bone cell survival by Pyk2 inhibition is achieved without altering bone renewal rate or bone biomechanical material properties. Hence, targeting the Pyk2/anoikis pathway represents a novel mechanistic approach to preserve skeletal integrity with GC excess, devoid of undesirable skeletal complications.

Materials and methods

Mice and tissue procurement.

Skeletally mature four-month old female mice with global deletion of Pyk2 (KO) and wild type littermate controls (WT) of C57BL/6 background were generated from breeders provided by Dr. Charles Turner, Indiana University, originally described in Okigaki et al. 2003 (24). Genotyping was performed by extracting genomic DNA from tissue samples, followed by PCR reaction using the following primers Pyk2 reverse (CCTGCTGGCAGCCTAACCACAT), Pyk2 wild type forward (GGAGGTCTATGAAGGTGTCTACACGAAC), and Pyk2 mutated forward (GCCAGCTCATTCCTCCCACTCAT). PCR products were run on an agarose gel with electrophoresis to distinguish the wild type and Pyk2 KO bands. Mice (5 per cage) were fed with a regular diet (Teklad Global 18% Protein Extruded Rodent Diet Sterilizable, Catalog number 2018SX, Harlan/ENVIGO, Indianapolis, IN, USA), received water *ad libitum*, and were maintained on a 12-h light/dark cycle in polycarbonate cages at the Laboratory Animal Research Center (LARC), at Indiana University School of Medicine. Mice were implanted with slow-release pellets delivering placebo, 1.4 mg/kg/d (GC1), or 2.1 mg/kg/d (GC2) prednisolone (Innovative Research of America, Sarasota, FL, USA) for four weeks (25). Previous studies showed that these doses reproduce in the mouse the hallmarks of GC-induced osteoporosis and are equivalent to medium and high therapeutic glucocorticoid doses in humans (25;26). C57BL/6 four-month old female mice were injected with vehicle or 10 mg/kg of the Pyk2/FAK inhibitor PF-431396 (PF) (Tocris Bioscience, Bristol, UK) five times per week, as previously published (27), beginning three days prior to placebo or GC2 pellet implantation for two weeks. To measure the dynamic histomorphometric indexes mineralizing surface to bone surface (MS/BS), mineral apposition rate (MAR), and bone formation rate normalized to bone surface (BFR/BS), KO and WT mice were injected 10 and 3 days prior to sacrifice with calcein (30 mg/kg, Sigma-Aldrich, St. Louis, MO, USA) and alizarin red (50 mg/kg, Sigma-Aldrich, St. Louis, MO, USA) solutions, respectively. The use of two different colors of fluorochromes permits the unequivocal identification of first and second labels and increases accuracy in the measurement of the distance between the two labels required for MAR calculation. Mice were euthanized by first sedation with 2% isoflurane (Abbott Laboratories, Chicago, IL, USA) administered by a Drager 19.1 Anesthetic Vaporizer, and then followed by cervical dislocation. Bones were dissected and processed as indicated below, and muscles were also dissected and weighed. Analysis was performed in a blinded fashion. All animal procedures were approved by the Institutional Animal

Care and Use Committee (IACUC) of Indiana University School of Medicine, and animal care was carried out in accordance with institutional guidelines.

BMD measurement and micro-CT analysis.
Lean body mass and BMD of the total body excluding the head and the tail, the lumbar spine (L1-L6), and the femur were measured by dual energy X-ray absorptiometry (DXA) scanning by using a PIXImus II densitometer (GE Medical Systems, Lunar Division, Madison, WI, USA). DXA measurements were performed 2-4 days before (initial) and 14 or 28 days (final) after pellet implantation (25;28). Mice were randomized to the experimental groups based on initial spine BMD. Briefly, mice were sorted by spinal BMD starting from the highest BMD, and then randomly distributed to the treatment groups. After randomization, no statistical differences on spinal BMD were found between experimental groups.
For micro-CT analysis, L6 vertebral and femoral bones were cleaned of soft tissue, fixed in 10% buffered formalin, and stored in 70% ethanol until scanned. Vertebrae were scanned at 6-μm resolution (Skyscan 1172, SkyScan, Aartselaar, Belgium) and femoral bones were scanned at 10-μm resolution (SCANCO 35, SCANCO Medical, Brüttisellen, Switzerland) and cancellous bone measurements were done 60 μm away from the growth plates as previously described (29). Cortical bone of the midshaft femur was performed for a 0.2 mm region located at the calculated femoral midpoint. The nomenclature for micro-CT indexes follows the guidelines previously recommended (30).

Mechanical testing.
The mechanical properties of L6 vertebrae were determined by axial compression after removal of vertebral processes and the cranial and caudal endplates. Vertebral bodies were loaded at a rate of 0.5 mm/min until failure (100P225 Modular Test Machine, TestResources, Shakopee, MN, USA), as previously described (25). The mechanical properties of femoral mid-diaphysis were assessed by three-point bending using standard methods (31). Femurs were placed with the posterior side down upon the bottom support (9 mm wide) with the descending probe contacted with the central anterior surface and loaded at a rate of 2 mm/min until failure (100P225 Modular Test Machine, TestResources, Shakopee, MN, USA), as previously described (32). Structural or extrinsic properties (energy to ultimate force, ultimate force, and stiffness) of the vertebra or femur were derived from the load/displacement curves obtained during the vertebral compression or three-point bending tests, respectively. The material or intrinsic properties (toughness, ultimate stress, and Young's modulus or intrinsic stiffness) were derived from the structural properties, by taking into account the geometry and volume of the samples quantified by micro-CT, following the calculations previously published (31;33).

Apoptosis analysis.
Apoptosis of osteoblasts and osteocytes was detected by the transferase-mediated biotin-dUTP nick end-labeling (TUNEL) reaction (GeneCopoeia, Rockville, MD, USA) in undecalcified vertebral and femoral bone sections counterstained with 2% methyl green as previously described (34). Apoptosis of osteoclasts and marrow osteoclasts was detected in double stained TRAPase, to identify osteoclasts, and TUNEL, to identify apoptotic cells, in the cancellous bone region starting 300μm from the distal growth plate and ending 1100μm proximal to the distal growth plate of paraffin-embedded femora. The total number of TRAPase positive cells (TRAP +cells) was also quantified including multinucleated cells both on bone surfaces and in the marrow as well as TUNEL positive and negative, which was then normalized by both bone surface and marrow area. The number of live and TUNEL positive marrow osteoclasts was

normalized to the total marrow area. The prevalence of apoptotic osteoblasts, osteocytes, osteoclasts, and marrow osteoclasts was calculated by enumerating the total number and TUNEL positive cells exhibiting condense chromatin, nuclear fragmentation, or cell shrinkage.

Serum biochemistry.
Blood was collected 2 and 4 weeks after pellet implantation from the facial vein of 3-hour fasted mice. N-terminal propeptide of type I procollagen (P1NP) (35), C-terminal telopeptides of type I collagen (CTX) (36), and tartrate-resistant acid phosphatase form 5b (TRAP5b) (37) were measured using enzyme-linked immunosorbent assays (Immunodiagnostic Systems Inc., Gaithersburg, MD, USA) (25;28). Osteocalcin (OCN) (38) was measured using the Mouse Osteocalcin KIA Kit (Alfa Aesar, Tewksbury, MA, USA).

Bone histomorphometry.
A subset of 3-6 samples was studied. L1-3 vertebrae and femoral bones were fixed in 10% neutral buffered formalin and embedded undecalcified in methyl methacrylate as previously described (34). Dynamic histomorphometry measurements were performed 4-µm unstained bone sections under epifluorescence microscopy. Histomorphometric analysis was performed using OsteoMeasure High Resolution Digital Video System (OsteoMetrics, Decatur, GA, USA) interfaced to an Olympus BX51 fluorescence microscope (Olympus America Inc., Center Valley, PA, USA) (28). Osteoclasts were quantified on L2 lumbar vertebral by analyzing the whole vertebral body region and distal femoral by analyzing the femoral cancellous bone region (starting 300µm from the distal growth plate and ending 1100µm proximal to the distal growth plate) of thin sections stained for tartrate-resistant acid phosphatase (TRAPase) and counterstained with Toluidine Blue, as previously published (25;28). Osteoclasts were defined as TRAPase positive cells attached to bone with 2 or more nuclei, following standardized histomorphometry guidelines by the American Society for Bone and Mineral Research (39) and recent publications (40-42). Osteoclast number was calculated by dividing the total number of osteoclasts attached to bone surfaces by the total bone surface (number/mm); and osteoclast surface was calculated by dividing the bone surface covered by osteoclasts by total bone surface, and multiplied by 100 (in %). A marrow osteoclast was defined as a multinucleated TRAPase positive cell with 2 or more nuclei separated from the bone surface by at least one other cell. Marrow osteoclast number was calculated by dividing the total number of marrow osteoclasts by the marrow area (number/mm^2). Longitudinal sections of the distal femurs were stained for von Kossa and counterstained with McNeal, as previously described (28).

Quantitative PCR.
Total RNA was extracted from vertebral lumbar bones (L4) and quantitative PCR was performed as previously described (25). RNA was extracted with TRIzol (Invitrogen, Carlsbad, CA, USA), and cDNA was synthesized by using high capacity cDNA reverse transcription kit (Applied Biosystems Inc., Foster City, CA, USA). Primer and probe sets were from Applied Biosystems or from Roche Applied Science (Indianapolis, IN, USA). Relative mRNA expression was normalized to the housekeeping gene ribosomal protein, large P2 (Rplp2) using the ΔCt method. Ratios between genes of interest and housekeeping gene are expressed as fold change compared to WT mice receiving placebo.

Mineralization assay.
Primary osteoblastic cells were isolated from the neonatal calvarial bones of C57BL/6 mice, KO, or WT littermate control mice, and plated at 5,000 cells/cm^2 density in MEM Alpha medium with 10% fetal bovine serum and 1% penicillin/streptomycin as previously described (25;43).

Osteogenic medium was used after cultures reached confluence consisting of 50 μg/ml ascorbic acid and 10 mM β-glycerophosphate and treated with 1μM dexamethasone or the corresponding vehicle (ethanol), and Pyk2 inhibitor (PF-431396) or the corresponding vehicle (DMSO). Medium was replaced every 2-3 days, and mineralization was visualized using the OsteoImage Mineralization Assay Kit (Lonza Walkersville Inc., Walkersville, MD, USA) or Alizarin Red S (Sigma-Aldrich, St. Louis, MO, USA) staining (43). Mineralization was quantified using a microplate reader for Lonza staining (492/520 nm excitation/emission fluorescence) or for Alizarin Red S staining (405 nm absorbance) (25;43).

Osteoclast apoptosis assay in vitro.
Bone marrow cells were flushed with sterile PBS from tibiae and femora of C57BL/6 mice or WT and KO mice and cultured in MEM Alpha medium with 10% fetal bovine serum and 1% penicillin/streptomycin for 48 hours, as previously described (17). Non-adherent cells were collected, re-plated at 300,000 cells/cm^2 density and differentiated with 80 ng/ml recombinant murine soluble RANKL (PeproTech, Rocky Hill, NJ, USA) and 20 ng/ml recombinant murine M-CSF (PeproTech, Rocky Hill, NJ, USA) for 4-6 days. Medium was replaced every 2 days and cells were treated with 10^{-5}M alendronate or corresponding vehicle (PBS) one hour prior to 1μM dexamethasone or the corresponding vehicle (EtOH) addition. After 24 hours, cells were fixed with 10% buffered formalin, rinsed with dH_2O, and stained for TRAPase (Sigma-Aldrich, St. Louis, MO, USA) with hematoxylin counterstaining. Apoptotic osteoclasts were identified by the presence of morphologic characteristics such as the loss of cell membrane integrity, nuclear condensation, and fragmentation.

Statistical analysis.
Data are expressed as means ± standard deviations (SD). Sample differences were evaluated using SigmaPlot 12.0 (Systat Software, Inc., San Jose, CA, USA). Statistically identified outliers for particular end points (value ± 2 times SD from the mean) were removed. Data of the *in vivo* and *in vitro* experiments were analyzed by two-way ANOVA using genotype (WT vs KO) or intervention (vehicle vs PF-431396) and treatment (placebo vs glucocorticoid) as independent variables. For apoptotic osteoclasts *in vitro* assays, a three-way ANOVA was used for genotype (WT vs KO) or intervention (vehicle vs PF-431396), treatment (vehicle vs dexamethasone), and apoptotic agent (vehicle vs alendronate). When ANOVA detected a significant interaction between the variables or a significant main effect, the post-hoc test Tukey was used to determine the significance of the effect of the treatment within each genotype or intervention condition.

Study approval.
All animal procedures were approved by the Institutional Animal Care and Use Committee of Indiana University School of Medicine, and animal care was carried out in accordance with institutional guidelines.

Results

Genetic deletion of Pyk2 protects from GC-induced loss of bone mass and strength, and osteoblast/osteocyte apoptosis, but not from the suppression of bone formation.
Mice lacking Pyk2 (KO) display higher bone mass at all sites, measured by DXA (**Figure 1A**); and increased vertebral (L6) cancellous bone (BV/TV), trabecular thickness (Tb.Th), trabecular number (Tb.N), and decreased trabecular separation (Tb.Sp), quantified by micro-CT (**Figure 1B-C**), consistent with previous reports (27;44). In WT mice, administration of two different doses of the GC prednisolone (GC1=1.4 or GC2=2.1 mg/kg/d) decreased total, spine, and femur

BMD (**Figure 1A**) and trabecular thickness (**Figure 1B-C**). The higher GC dose also decreased cancellous BV/TV in WT mice (**Figure 1C**, left graph). In contrast, KO mice were resistant to GC effects on bone mass and volume (**Figure 1A-C**). WT and KO littermate mice exhibit similar body weight that was not altered by GC (not shown), and similar lean body mass that was reduced by GC similarly in both genotypes (**Figure 2A**). In addition, the weight of tibialis anterior and gastrocnemius muscles was decreased by GC to a similar extent in WT and KO mice (**Figure 2B**).

KO mice also exhibited enhanced structural (or extrinsic) mechanical properties of ultimate force, energy to ultimate load, and stiffness, measured in vertebral bone compared to WT mice (**Table 1**). However, no differences in material (or intrinsic) mechanical properties (toughness, ultimate stress, and Young's modulus) were detected between the two genotypes. These findings suggest that the gain in bone strength in KO mice is due to increased bone mass and not to alterations at the tissue level (i.e. mineralization or collagen structure). GC treatment decreased the structural properties of ultimate force and energy to ultimate load, as well as the material property of toughness in WT mice (**Figure 1D**). In contrast, KO mice were protected from any changes in structural or material mechanical properties induced by GC.

We next examined the underlying mechanism of the protection from GC-induced bone loss by Pyk2 deletion. Overall, deletion of Pyk2 under basal conditions did not alter osteoblast or osteocyte apoptosis, circulating levels of formation and remodeling markers (P1NP or OCN, respectively), or dynamic histomorphometric parameters (MS/BS, MAR, and BFR/BS), except for a decrease in P1NP exhibited by KO mice detected at 4 weeks but not at 2 weeks after pellet implantation (**Figure 1E-H**). GC induced the expected increase in osteoblast and osteocyte apoptosis in cancellous and cortical bone in WT mice, whereas KO mice were protected (**Figure 1E**). This finding is consistent with the previous demonstration that Pyk2 kinase expression and activity is required for GC-induced apoptosis of osteocytic cells *in vitro* (23). However, KO mice were not protected from the reduction of bone formation induced by GC. Thus, GC decreased serum P1NP and OCN in both WT and KO mice (**Figure 1F-G**); and decreased MS/BS, MAR, and BFR/BS to the same extent in WT and KO mice (**Figure 1H**). GC reduced the mRNA expression of osteocalcin, collagen 1a1, and alkaline phosphatase in bones from both WT and Pyk2 KO mice (**Figure 1I**). This persistent inhibitory effect of GC on the biosynthetic activity of osteoblasts in the KO mice explains the inability of Pyk2 inhibition to prevent the decreased bone formation induced by the hormones.

Short-term pharmacologic Pyk2 inhibition prevents GC-induced bone loss, fragility, and osteoblast/osteocyte apoptosis, but not the suppression of bone formation.

Consistent with the musculoskeletal response of KO mice, pharmacologic inhibition of Pyk2 with the kinase inhibitor PF-431396 (PF) prevented the loss of BMD induced by short-term (2 weeks) treatment with GC (**Figure 3A**). In contrast, and similar to the genetic deletion of Pyk2, PF did not prevent the loss of lean body mass or the mass of individual muscles induced by GC (**Figure 2A** and **B**). PF-treated mice were also protected from GC-induced deterioration of femoral bone microarchitecture, specifically from trabecular and cortical thinning (**Figure 3B-C**). PF prevented the reduction induced by GC in the cortical area fraction (Ct.Ar/Tt.Ar), which was mainly driven by the loss of cortical bone area (Ct.Ar) from the endosteal bone surface as no reductions in the cortical bone total cross-sectional area (Tt.Ar) were detected. PF also prevented the decreases in ultimate force, energy to ultimate load, and toughness induced by GC (**Figure 3D** and **Table 2**).

The 2-week treatment with GC induced the expected increase in osteoblast and osteocyte apoptosis in cancellous and cortical bone in vehicle-treated mice, but not in PF-treated mice (**Figure 3E**). PF alone did not affect osteoblast/osteocyte apoptosis, but increased circulating P1NP and osteoblast number and surface compared to vehicle-treated mice (**Figure 3F-G**). However, all GC-treated mice exhibited similar reductions in P1NP, OCN, osteoblast number, and osteoblast surface regardless of PF administration when compared to respective placebo controls, demonstrating that GC affect osteoblast number and function independently of Pyk2 activity (similar to genetic deletion of Pyk2 shown in **Figure 1**).

Consistent with these *in vivo* effects of GC, addition of the synthetic GC dexamethasone decreased hydroxyapatite deposition to a similar extent in primary cultures of calvarial osteoblasts derived from WT or KO mice (**Figure 3H**); and decreased calcium deposition in the absence or presence of PF (**Figure 3I**). Further, mineral deposition was increased in cultures of KO-derived osteoblasts or osteoblasts treated with PF alone compared to the respective controls (**Figure 3H-I**), mimicking the increase in P1NP (**Figure 3F**) and in osteoblast number and surface (**Figure 3G**) exhibited by PF-treated mice. These findings are consistent with the increase in BFR/BS, MAR, MS/BS induced by PF in ovariectomized rats previously reported (27). These findings demonstrate that Pyk2 deletion/inhibition increases osteoblast activity under basal conditions but cannot overcome GC-induced decrease in matrix mineral production or bone formation.

Loss of Pyk2 signaling by genetic or pharmacologic means protects from GC-induced bone resorption by decreasing activity of individual osteoclasts and promoting osteoclast detachment from bone.

We next examine the effects of Pyk2 deletion/inhibition on GC-induced bone resorption. Circulating levels of the resorption marker CTX were not affected by genetic deletion of Pyk2 (**Figure 4A**). However, KO mice exhibited increased circulating levels of TRAP5b, an index of osteoclast number (**Figure 4B**). As a consequence, KO mice exhibited lower CTX/TRAP5b ratio, which indicates decreased activity of individual osteoclasts (**Figure 4C**). Consistent with normal CTX levels in KO mice, the number of osteoclasts or the bone surface covered by osteoclasts quantified by histomorphometry was not different in KO compared to WT mice (**Figure 4D,** left and middle panels). However, KO mice exhibited approximately a 3-fold increase in the number of osteoclasts present in the bone marrow compared to WT, consistent with the increased TRAP5b in the circulation. Therefore, KO mice exhibited increased number of inactive osteoclasts detached from the bone surface explaining the mismatch between the low CTX/TRAP5b ratio.

Both doses of GC induced the expected increase in CTX and TRAP5b in WT mice (**Figure 4A-B**). However, GC did not affect CTX or further increase the already elevated circulating TRAP5b levels in KO mice. Moreover, GC did not change the CTX/TRAP5b ratio in either WT or KO mice (**Figure 4C**), suggesting that increased resorption induced by GC in WT mice is due to an increase in osteoclast number but not in the activity of individual osteoclasts. Indeed, GC increased osteoclast number in bone in both WT and KO mice, but GC increased osteoclast surface only in WT mice (**Figure 4D,** left and middle panels). Consistent with increased osteoclast number in the marrow (**Figure 4D**, right panel), mRNA expression of TRAPase as well as cathepsin K is increased in vertebral bone/bone marrow preparations from KO mice (**Figure 4E**). This finding demonstrates that osteoclasts in the marrow also express cathepsin K as the majority of osteoclasts in the KO mice are present in the marrow. Close examination of bone sections showed that osteoclasts were fully attached to bone in GC-treated WT mice,

(**Figure 4F**, top images). In contrast, osteoclasts were only partially attached in GC-treated KO mice (**Figure 4F**, bottom images). Cartoons and representative images of WT and KO osteoclasts are shown in **Figure 4G**. The difference in osteoclast attachment to bone surfaces explains the apparent discrepancy between osteoclast number and surface in response to GC in WT versus KO mice.

The protection from bone loss induced by GC by genetic deletion of Pyk2 was reproduced by short-term blockade of Pyk2 kinase activity with the pharmacological inhibitor PF-431396 (PF). Two weeks of GC treatment increased CTX, TRAP5b, and osteoclast number and surface in vehicle-treated mice (**Figure 4H** and **I**). PF did not alter any of these parameters in placebo treated mice. However, PF inhibited the increase in CTX and osteoclast number/surface induced by GC. In contrast, PF did not inhibit the increase in TRAP5b induced by GC. Moreover, similar to genetic deletion of Pyk2, treatment with PF increased the number of osteoclasts in the marrow, which were further elevated in mice treated with both PF and GC.

Decreased GC-induced resorption by genetic or pharmacologic inhibition of Pyk2 is due to osteoclast apoptosis, which overrides the prosurvival effects of GC on osteoclasts.

The impaired attachment to bone of osteoclasts from KO or PF-treated mice was due to premature death by apoptosis, as evidenced by increased prevalence of apoptotic osteoclasts (TUNEL and TRAPase positive) on bone surfaces as well as in the bone marrow in bones from KO or from PF-treated mice compared to respective controls (**Figure 5A-B**). These findings strongly suggest that the reduction in osteoclast function by inhibition of Pyk2 signaling *in vivo* is due to detachment-induced apoptosis (i.e. anoikis).

GC did not alter the increased osteoclast apoptosis in bone from either KO or PF-treated mice. However, mice treated with GC and the PF inhibitor exhibited a higher prevalence of apoptotic osteoclasts in the marrow compared to mice treated with PF alone. This effect paralleled the increased TRAP5b induced by GC (**Figure 4H**), suggesting that the increased osteoclasts generated by GC undergo premature apoptosis induced by PF and are unable to reach the bone surfaces, thus accumulating in the marrow.

Increased apoptosis is an intrinsic feature of osteoclasts from KO mice, as it was evidenced *in vitro* in osteoclast precursors derived from KO mice cultured in the presence of RANKL and M-CSF (**Figure 5C**). Osteoclasts in these cultures exhibited abnormal morphology, impaired spreading, and absence of organized podosomes (**Figure 5D**), consistent with previous reports using immunofluoresecence microscopy to detect F-actin and tubulin and depicting morphologic defects of Pyk2 deficient osteoclasts *in vitro* (44). Moreover, KO osteoclast cultures exhibited a reduction in the total number of TRAPase positive cells with 3 or more nuclei (898 ± 238 vs 309 ± 249, WT vs KO respectively), suggesting that impaired attachment leads to premature apoptosis (i.e. anoikis). This phenomenon could explain the decreased activity of individual osteoclasts *in vivo* evidenced by a lower CTX/TRAP5b ratio (**Figure 4C**).

Earlier findings showed that prolongation of the lifespan of preexisting osteoclasts explains part of the increase in bone resorption induced by GC (17;18). This anti-apoptotic effect of GC was readily demonstrated in cultures of osteoclasts derived from WT mice treated with the bisphosphonate (BP) alendronate (indicated by **#** in **Figure 5C** and images shown in **Figure 5D**). Thus, BP treatment increased apoptosis of TRAPase positive cells either with ≥3 nuclei or <3 nuclei, which was prevented by dexamethasone by 60% and 46%, respectively. However, the survival effect of dexamethasone was absent in osteoclasts derived from KO mice. Further, whereas dexamethasone prevented BP-induced apoptosis in WT osteoclast cultures treated with vehicle by 51%, it was ineffective in cultures treated with the Pyk2 inhibitor PF (**Figure 5E-F**),

although PF addition did not significantly altered total number of TRAPase positive cells (1101 ± 280 vs 907 ± 144, veh vs PF, respectively). Taken together, these pieces of evidence demonstrate that prolongation of osteoclast lifespan by GC is negated in the absence of Pyk2 expression/activity and, thus, the inherent osteoclast dysfunction and increased osteoclast apoptosis conferred by lack of Pyk2 overrides GC-induced resorption.

Discussion

We identified in the current studies the Pyk2/anoikis signaling pathway as a new therapeutic target that opposes GC effects on bone cells. Pyk2 activation is required for GC to induce apoptosis of osteoblasts and osteocytes and to prolong the lifespan of osteoclasts, leading to increased resorption. Either genetic deletion or short-term pharmacologic inhibition of Pyk2 overrides GC regulation of bone cell anoikis, maintaining osteoblast/osteocyte viability while shortening osteoclast lifespan. Remarkably, Pyk2 inhibition prevents bone loss primarily by inhibiting resorption and interfering with osteoclast survival induced by GC, as bone formation is still suppressed even when osteoblast apoptosis induced by GC is prevented by Pyk2 inhibition. Importantly, inhibiting Pyk2 signaling bypasses the negative effects of the current standard of care, thus preserving bone renewal rate and the biomechanical material properties of bone. We conclude that targeting the Pyk2/anoikis pathway represents a novel mechanistic approach to maintain skeletal integrity with GC excess (**Figure 6**).

Our studies reveal that the Pyk2 kinase is at the core of the mechanism underlying the opposing regulation of apoptosis by GC depending on the bone cell lineage, a hallmark of GC action. Whereas Pyk2 phosphorylation induced by GC promotes apoptosis of osteoblasts and osteocytes, it stimulates podosome formation and induces attachment of osteoclasts to bone surfaces, prolonging osteoclast lifespan. Consequently, genetic absence of Pyk2 or treatment with a Pyk2 inhibitor prevented GC effects on bone cell anoikis maintaining osteoblast/osteocyte viability and at the same time promoting osteoclast apoptosis.

A remarkable feature of the Pyk2/anoikis pathway is that its pharmacologic inhibition rapidly inhibits bone resorption stimulated by GC by inducing osteoclast detachment from bone and apoptosis of osteoclasts, which accumulate in the marrow. This mechanism could potentially be exploited to block bone loss in other pathological conditions in which osteoclast production is exaggerated. In particular, inhibitors of Pyk2/anoikis signaling could also potentially block the bone loss associated with aging, which is another leading cause of osteoporosis world-wide. GC activity is regulated by two isoforms of 11β-hydroxysteroid dehydrogenase (11β-HSD): 11β-HSD1 that converts inactive (cortisone) to active (cortisol) metabolites and 11β-HSD2 that catalyzes the opposite reaction (45). The level of expression of 11β-HSD1 predicts the severity of the skeletal response to GC action (46) and also increases with age (47). Thus, exaggerated endogenous GC activity likely contributes to the mechanism underlying age-related bone loss, and interventions that prevent iatrogenic GC-induced bone disease could also ameliorate the skeletal fragility due to aging.

Unlike bisphosphonates and denosumab (RANKL antibody), also used to manage GC-induced osteoporosis (9-12;48), targeting the Pyk2/anoikis pathway decreased bone resorption to placebo levels without severely reducing bone turnover, and did not further suppress bone formation below the already low rate induced by GC. Thus, inhibition of the Pyk2/anoikis pathway represents an alternative approach to effectively reduce GC-induced resorption, while circumventing the side-effects associated with potent anti-resorptive agents.

Apoptosis of osteoblasts induced by GC is prevented by Pyk2 inhibition. However, bone formation is still suppressed in the KO mice or in mice treated with the Pyk2 inhibitor. These findings suggest minimal, if any, contribution of apoptosis to osteoblast function in the frame of GC excess. This outcome is not surprising, considering the pleiotropic effects of the hormones, which affect osteoblast function by several mechanisms. Indeed, in mice with Pyk2 genetic deletion, GC still inhibited the synthetic activity of osteoblasts as evidenced by the reduction in osteocalcin, collagen 1a1, and alkaline phosphatase expression. These findings demonstrate that Pyk2 inhibition specifically interferes with the regulation of osteoblast anoikis by GC, whereas GC inhibition of bone formation and mineral matrix production in osteoblasts occurs independently of Pyk2. Future investigations are required to examine the efficacy of Pyk2 inhibition in long term experiments in which bone loss induced by GC is primarily driven by the reduction in bone formation induced by the hormones.

Maintenance of osteocyte viability with Pyk2 inhibition could contribute to preservation of bone strength in our studies, as previous reports demonstrated that prevention of osteocyte apoptosis by genetic means preserves at least part of bone strength even when GC induce loss of bone mineral (15). Future studies are warranted to examine whether long term inhibition of Pyk2 activity prevents the development of osteonecrosis, a process that has been linked to GC-induced osteocyte apoptosis (49).

Because of bone and muscle act as a mechanical unit, it could be expected that changes in one tissue might impact the other. However, in contrast to the observed bone protection, KO or PF-treated mice still exhibited muscle wasting induced by GC. These findings show a lack of crosstalk between these two tissues in the context of GC excess and also demonstrate that the effects of the GC on skeletal muscle are independent of Pyk2 expression or activity. One mechanism by which bone might influence muscle is through growth factors stored in the bone matrix. In particular, TGF-β released into the circulation by the process of bone resorption has been implicated in the oxidation and nitrosylation of the ryanodine receptor and calcium release channel (RyR1) in skeletal muscle leading to muscle weakness in cancer (50). Our findings in which Pyk2 inhibition effectively blocks resorption but does not alter muscle atrophy argue against this mechanism in the context of GC excess. Similarly, blocking GC-induced resorption by genetic deletion of Sost/sclerostin does not protect muscle (25). Taken together, this evidence highlights the need for therapeutic interventions that simultaneously interfere with the damaging actions of GC in both bone and muscle.

In conclusion, targeting the Pyk2/anoikis pathway represents a novel mechanistic approach to preserve skeletal integrity in glucocorticoid excess, devoid of undesirable skeletal complications.

National Institute of Arthritis and Musculoskeletal and Skin Diseases http://dx.doi.org/10.13039/100000069, R01-AR059357, Teresita Bellido; National Institutes of Health http://dx.doi.org/10.13039/100000002, T32-AR065971, Amy Y Sato; Veterans Administration, I01 BX002104, Teresita Bellido

Acknowledgements

The authors thank members of the Bellido lab for assistance in tissue collection and Drs. Munro Peacock and Jesus Delgado-Calle for critical reading of the manuscript. This research was supported by the National Institutes of Health (R01-AR059357 to T.B.; T32-AR065971 to A.Y.S.) and the Veterans Administration (I01 BX002104 to T.B.).

Author contributions: T.B. conceptualization, experimental design, resources, formal analysis, supervision, project administration, manuscript writing and editing; A.Y.S.: experiments

execution, data acquisition, initial data analysis, first manuscript draft writing; M.C., K.M., K.W.C., and T.L.: data acquisition and initial analysis; L.I.P.: assistance with data interpretation, figure drawing, and methodology writing. All authors reviewed and approved the manuscript before submission.

Corresponding author and person to whom reprint requests should be addressed: Teresita Bellido, PhD, Department of Anatomy and Cell Biology and Department of Internal Medicine, Endocrinology, Indiana University School of Medicine, 635 Barnhill Drive, MS5045A; Indianapolis, IN 46202, USA, Phone: 317-274-7410, Fax: 317-278-2040, email: tbellido@iupui.edu

Disclosure Statement:
The authors have nothing to disclose.

Reference List

1. **Rhen T, Cidlowski JA** 2005 Antiinflammatory action of glucocorticoids--new mechanisms for old drugs. N Engl J Med 353:1711-1723
2. **Necela BM, Cidlowski JA** 2004 Mechanisms of glucocorticoid receptor action in noninflammatory and inflammatory cells. Proc Am Thorac Soc 1:239-246
3. Rizzoli R, Adachi JD, Cooper C, Dere W, Devogelaer JP, Diez-Perez A, Kanis JA, Laslop A, Mitlak B, Papapoulos S, Ralston S, Reiter S, Werhya G, Reginster JY 2012 Management of glucocorticoid-induced osteoporosis. Calcif Tissue Int 91:225-243
4. **Weinstein RS** 2011 Clinical practice. Glucocorticoid-induced bone disease. N Engl J Med 365:62-70
5. **Van Staa TP** 2006 The pathogenesis, epidemiology and management of glucocorticoid-induced osteoporosis. Calcif Tissue Int 79:129-137
6. **Littooij AS, Kwee TC, Enriquez G, Verbeke JI, Granata C, Beishuizen A, de LC, Zennaro F, Bruin MC, Nievelstein RA** 2017 Whole-body MRI reveals high incidence of osteonecrosis in children treated for Hodgkin lymphoma. Br J Haematol 176:637-642
7. **Ross EJ, Linch DC** 1982 Cushing's syndrome--killing disease: discriminatory value of signs and symptoms aiding early diagnosis. Lancet 2:646-649
8. **Van Staa TP, Leufkens HGM, Abenhaim L, Zhang B, Cooper C** 2000 Use of oral corticoisteroids and risk of fractures. J Bone Min Res 15:993-1000
9. **Davis K, Neese K., Sood A** 2018 FDA approves prolia (denosumab) for glucocorticoid-induced osteoporosis. Amgen, Retrieved from URL.: https://www.amgen.com/media/news-releases/2018/05/fda-approves-prolia-denosumab-for-glucocorticoidinduced-osteoporosis/
10. Saag KG, Emkey R, Schnitzer TJ, Brown JP, Hawkins F, Goemaere S, Thamsborg G, Liberman UA, Delmas PD, Malice MP, Czachur M, Daifotis AG 1998 Alendronate for the prevention and treatment of glucocorticoid-induced osteoporosis. Glucocorticoid-Induced Osteoporosis Intervention Study Group. N Engl J Med 339:292-299
11. **Mok CC, Ho LY, Ma KM** 2015 Switching of oral bisphosphonates to denosumab in chronic glucocorticoid users: a 12-month randomized controlled trial. Bone 75:222-228
12. **Saag KG, Shane E, Boonen S, Marin F, Donley DW, Taylor KA, Dalsky GP, Marcus R** 2007 Teriparatide or alendronate in glucocorticoid-induced osteoporosis. N Engl J Med 357:2028-2039

13. **Allen MR, Burr DB** 2007 Mineralization, Microdamage, and Matrix: How Bisphosphonates Influence Material Properties of Bone. BoneKEy-osteovision 4:49-60

14. **O'Ryan FS, Khoury S, Liao W, Han MM, Hui RL, Baer D, Martin D, Liberty D, Lo JC** 2009 Intravenous bisphosphonate-related osteonecrosis of the jaw: bone scintigraphy as an early indicator. J Oral Maxillofac Surg 67:1363-1372

15. **O'Brien CA, Jia D, Plotkin LI, Bellido T, Powers CC, Stewart SA, Manolagas SC, Weinstein RS** 2004 Glucocorticoids act directly on osteoblasts and osteocytes to induce their apoptosis and reduce bone formation and strength. Endocrinology 145:1835-1841

16. **Jia D, O'Brien CA, Stewart SA, Manolagas SC, Weinstein RS** 2006 Glucocorticoids act directly on osteoclasts to increase their lifespan and reduce bone density. Endocrinology 147:5592-5599

17. **Weinstein RS, Chen JR, Powers CC, Stewart SA, Landes RD, Bellido T, Jilka RL, Parfitt AM, Manolagas SC** 2002 Promotion of osteoclast survival and antagonism of bisphosphonate-induced osteoclast apoptosis by glucocorticoids. J Clin Invest 109:1041-1048

18. **Sato AY, Peacock M, Bellido T** 2018 Glucocorticoid excess in bone and muscle. Clinical Reviews in Bone and Mineral Metabolism 16:33-47

19. **Bellido T, Plotkin LI, Bruzzaniti A** 2014 Bone cells. In: Burr D, Allen MR, eds. Basic and Applied Bone Biology. First ed. Elsevier Inc.; 27-45

20. **Parfitt AM** 1996 Skeletal heterogeneity and the purposes of bone remodeling. Osteoporosis. San Diego: Academic Press; 315-329

21. **Jilka RL, Bellido T, Almeida M, Plotkin LI, O'Brien CA, Weinstein RS, Manolagas SC** 2008 Apoptosis in bone cells. In: Bilezikian JP, Raisz LG, Martin TJ, eds. Principles of Bone Biology. 3er ed. San Diego, San Francisco, New York, London, Sydney, Tokyo: Academic Press; 237-261

22. **Zhao H, Ross FP, Teitelbaum SL** 2005 Unoccupied alpha(v)beta3 integrin regulates osteoclast apoptosis by transmitting a positive death signal. Mol Endocrinol 19:771-780

23. **Plotkin LI, Manolagas SC, Bellido T** 2007 Glucocorticoids induce osteocyte apoptosis by blocking focal adhesion kinase-mediated survival: evidence for inside-out signaling leading to anoikis. J Biol Chem 282:24120-24130

24. **Okigaki M, Davis C, Falasca M, Harroch S, Felsenfeld DP, Sheetz MP, Schlessinger J** 2003 Pyk2 regulates multiple signaling events crucial for macrophage morphology and migration. Proc Natl Acad Sci U S A 100:10740-10745

25. **Sato AY, Cregor M, Delgado-Calle J, Condon KW, Allen MR, Peacock M, Plotkin LI, Bellido T** 2016 Protection from glucocorticoid-induced osteoporosis by anti-catabolic signaling in the absence of Sost/sclerostin. J Bone Miner Res 31:1791-1802

26. **Weinstein RS, Jilka RL, Parfitt AM, Manolagas SC** 1998 Inhibition of osteoblastogenesis and promotion of apoptosis of osteoblasts and osteocytes by glucocorticoids: potential mechanisms of their deleterious effects on bone. J Clin Invest 102:274-282

27. Buckbinder L, Crawford DT, Qi H, Ke HZ, Olson LM, Long KR, Bonnette PC, Baumann AP, Hambor JE, Grasser WA, Pan LC, Owen TA, Luzzio MJ, Hulford CA, Gebhard DF, Paralkar VM, Simmons HA, Kath JC, Roberts WG, Smock SL, Guzman-Perez A, Brown TA, Li M 2007 Proline-rich tyrosine kinase 2 regulates osteoprogenitor cells and bone formation, and offers an anabolic treatment approach for osteoporosis. Proc Natl Acad Sci U S A 104:10619-10624

28. **Tu X, Delgado-Calle J, Condon KW, Maycas M, Zhang H, Carlesso N, Taketo MM, Burr DB, Plotkin LI, Bellido T** 2015 Osteocytes mediate the anabolic actions of canonical Wnt/β-catenin signaling in bone. Proc Natl Acad Sci U S A 112:E478-E486

29. **Rhee Y, Allen MR, Condon K, Lezcano V, Ronda AC, Galli C, Olivos N, Passeri G, O'Brien CA, Bivi N, Plotkin LI, Bellido T** 2011 PTH receptor signaling in osteocytes governs periosteal bone formation and intra-cortical remodeling. J Bone Miner Res 26:1035-1046

30. **Bouxsein ML, Boyd SK, Christiansen BA, Guldberg RE, Jepsen KJ, Muller R** 2010 Guidelines for assessment of bone microstructure in rodents using micro-computed tomography. J Bone Miner Res 25:1468-1486

31. **Turner CH, Burr DB** 1993 Basic biomechanical measurements of bone: a tutorial. Bone 14:595-608

32. **Hill Gallant KM, Gallant MA, Brown DM, Sato AY, Williams JN, Burr DB** 2014 Raloxifene prevents skeletal fragility in adult female Zucker Diabetic Sprague-Dawley rats. PLoS ONE 9:e108262

33. **Allen MR, Iwata K, Phipps R, Burr DB** 2006 Alterations in canine vertebral bone turnover, microdamage accumulation, and biomechanical properties following 1-year treatment with clinical treatment doses of risedronate or alendronate. Bone 39:872-879

34. **Plotkin LI, Weinstein RS, Parfitt AM, Roberson PK, Manolagas SC, Bellido T** 1999 Prevention of osteocyte and osteoblast apoptosis by bisphosphonates and calcitonin. J Clin Invest 104:1363-1374

35. **RRID:AB_2801263,** https://scicrunch.org/resolver/AB_2801263

36. **RRID:AB_2801265,** https://scicrunch.org/resolver/AB_2801265

37. **RRID:AB_2801266,** https://scicrunch.org/resolver/AB_2801266

38. **RRID:AB_2801264,** https://scicrunch.org/resolver/AB_2801264

39. **Dempster DW, Compston JE, Drezner MK, Glorieux FH, Kanis JA, Malluche H, Meunier PJ, Ott SM, Recker RR, Parfitt AM** 2013 Standardized nomenclature, symbols, and units for bone histomorphometry: A 2012 update of the report of the ASBMR Histomorphometry Nomenclature Committee. J Bone Miner Res 28:2-17

40. **Shiwaku Y, Neff L, Nagano K, Takeyama K, de BJ, Dard M, Gori F, Baron R** 2015 The Crosstalk between Osteoclasts and Osteoblasts Is Dependent upon the Composition and Structure of Biphasic Calcium Phosphates. PLoS ONE 10:e0132903

41. **Hajjawi MO, MacRae V, Huesa C, Boyde A, Millan JL, Arnett TR, Orriss IR** 2014 Mineralisation of collagen rich soft tissues and osteocyte lacunae in Enpp1 mice. Bone

42. **Wilson SR, Peters C, Saftig P, Bromme D** 2009 Cathepsin K activity-dependent regulation of osteoclast actin ring formation and bone resorption. J Biol Chem 284:2584-2592

43. **Sato AY, Tu X, McAndrews KA, Plotkin LI, Bellido T** 2015 Prevention of glucocorticoid induced-apoptosis of osteoblasts and osteocytes by protecting against endoplasmic reticulum (ER) stress in vitro and in vivo in female mice. Bone 73:60-68

44. **Gil-Henn H, Destaing O, Sims NA, Aoki K, Alles N, Neff L, Sanjay A, Bruzzaniti A, De Camilli P, Baron R, Schlessinger J** 2007 Defective microtubule-dependent podosome organization in osteoclasts leads to increased bone density in Pyk2(-/-) mice. J Cell Biol 178:1053-1064

45. **Tomlinson JW, Walker EA, Bujalska IJ, Draper N, Lavery GG, Cooper MS, Hewison M, Stewart PM** 2004 11beta-hydroxysteroid dehydrogenase type 1: a tissue-specific regulator of glucocorticoid response. Endocr Rev 25:831-866

46. **Cooper MS, Blumsohn A, Goddard PE, Bartlett WA, Shackleton CH, Eastell R, Hewison M, Stewart PM** 2003 11beta-hydroxysteroid dehydrogenase type 1 activity predicts the effects of glucocorticoids on bone. J Clin Endocrinol Metab 88:3874-3877

47. **Cooper MS, Rabbitt EH, Goddard PE, Bartlett WA, Hewison M, Stewart PM** 2002 Osteoblastic 11beta-hydroxysteroid dehydrogenase type 1 activity increases with age and glucocorticoid exposure. J Bone Miner Res 17:979-986

48. **Saag KG, Zanchetta JR, Devogelaer JP, Adler RA, Eastell R, See K, Krege JH, Krohn K, Warner MR** 2009 Effects of teriparatide versus alendronate for treating glucocorticoid-induced osteoporosis: thirty-six-month results of a randomized, double-blind, controlled trial. Arthritis Rheum 60:3346-3355

49. **Weinstein RS, Nicholas RW, Manolagas SC** 2000 Apoptosis of osteocytes in glucocorticoid-induced osteonecrosis of the hip. J Clin Endocrinol Metab 85:2907-2912

50. Waning DL, Mohammad KS, Reiken S, Xie W, Andersson DC, John S, Chiechi A, Wright LE, Umanskaya A, Niewolna M, Trivedi T, Charkhzarrin S, Khatiwada P, Wronska A, Haynes A, Benassi MS, Witzmann FA, Zhen G, Wang X, Cao X, Roodman GD, Marks AR, Guise TA 2015 Excess TGF-beta mediates muscle weakness associated with bone metastases in mice. Nat Med 21:1262-1271

Figure 1. Life-long genetic deletion of Pyk2 protects from GC-induced loss of bone mass and strength, and osteoblast/osteocyte apoptosis. (A) BMD for WT or KO mice treated with placebo, 1.4 mg/kg/d prednisolone (GC1), or 2.1 mg/kg/d prednisolone (GC2) for 28 days, measured by DXA. WT, N=10/10/9, placebo/GC1/GC2; KO N=10/9/7, placebo/GC1/GC2. **(B-C)** Bone volume fraction of bone volume/tissue volume (BV/TV), trabecular thickness (Tb.Th), number (Tb.N), and separation (Tb.Sp) of WT or KO lumbar vertebrae L6 are shown. WT, N=10/10/9, placebo/GC1/GC2; KO N=10/9/7, placebo/GC1/GC2. **(D)** Biomechanical properties were measured in vertebral bone (L6) by axial compression testing; WT, N=10/10/9, placebo/GC1/GC2; KO N=10/9/7, placebo/GC1/GC2. **(E)** Apoptosis of osteoblasts (Ob) and osteocytes (Ot) was quantified in cancellous and cortical bone in longitudinal sections of lumbar vertebrae (L1-L3) of WT or KO mice stained for TUNEL. WT, N=4/3/4, placebo/GC1/GC2; KO N=4/3/3, placebo/GC1/GC2. **(F-G)** P1NP, WT, N=10/10/10, placebo/GC1/GC2; KO N=8/10/10, placebo/GC1/GC2, and OCN, WT, N=7/7/6, placebo/GC1/GC2; KO N=7/6/6, placebo/GC1/GC2, were measured in blood samples collected 2 and 4 weeks after pellet implantation for WT or KO mice. **(H)** Mineralizing bone surface per bone surface (MS/BS), mineral apposition rate (MAR), and bone formation rate per bone surface (BFR/BS) were quantified in longitudinal sections of lumbar vertebra (L1-L3). WT, N=5/4/4, placebo/GC1/GC2; KO N=5/4/4, placebo/GC1/GC2. **(I)** Expression of indicated genes in L4 bones is shown, WT, N=8/8/8, placebo/GC1/GC2; KO N=8/8/8, placebo/GC1/GC2. Bars represent means ± SD. *p<0.05 vs corresponding placebo-treated mice and #p<0.05 vs placebo-treated WT mice, by two-way ANOVA, Tukey post-hoc test.

Figure 2. Pyk2 deficiency or inhibition does not prevent glucocorticoid induced muscle wasting. Lean body mass **(A)** and mass of isolated muscles normalized by body weight **(B)** are shown. WT, N=10/10/9, placebo/GC1/GC2; KO N=10/9/7, placebo/GC1/GC2; veh, N=9/9, placebo/GC2; PF N=10/6, placebo/GC2. *p<0.05 vs corresponding placebo-treated mice and #p<0.05 vs corresponding GC-treated WT mice by two-way ANOVA, Tukey post-hoc test.

Figure 3. Short-term pharmacologic Pyk2 inhibition prevents GC-induced bone loss, fragility, and osteoblast/osteocyte apoptosis. (A) BMD for vehicle (veh) or PF-431396 (PF) treated C57BL/6 mice implanted with placebo or 2.1 mg/kg/d prednisolone (GC2) for 14 days, measured by DXA. veh, N=9/9, placebo/GC2; PF N=10/6, placebo/GC2. **(B)** BV/TV, Tb.Th, Tb.N, and Tb.Sp of the distal femur of veh or PF-treated mice measured by micro-CT. veh, N=9/9, placebo/GC2; PF N=10/6, placebo/GC2. **(C)** Cortical area fraction (Ct.Ar/Tt.Ar), cortical bone area (Ct.Ar), total cross-sectional area (Tt.Ar), and cortical thickness (Ct.Th) of veh or PF-treated femoral midshafts are shown. veh, N=9/9, placebo/GC2; PF N=10/6, placebo/GC2. **(D)** Biomechanical properties were measured in the femoral mid-diaphysis by three-point bending. veh, N=9/9, placebo/GC2; PF N=10/6, placebo/GC2. **(E)** Osteoblasts (Ob) and osteocytes (Ot) apoptosis was quantified in cancellous and cortical bone in TUNEL stained longitudinal lumbar vertebrae (L1-L3) sections of veh or PF-treated mice. veh, N=5/5, placebo/GC2; PF N=5/3, placebo/GC2 N=3-5. **(F)** P1NP, veh, N=9/9, placebo/GC2; PF N=10/6, placebo/GC2, and OCN, veh, N=7/7, placebo/GC2; PF N=7/6, placebo/GC2, were measured in veh or PF-treated mice. **(G)** Osteoblast number (Ob.N/BS) and surface (Ob.S/BS) normalized to bone surface were measured in von Kossa/McNeal stained longitudinal distal femur sections. veh, N=3/3, placebo/GC2; PF N=3/4, placebo/GC2. **(H)** Quantification of mineralization in cultures of calvaria-derived primary osteoblastic cells from WT or KO mice treated with vehicle (veh) or dexamethasone (dex) and stained using the OsteoImage Mineralization Assay Kit. Scale bars: 400 μm. WT, N=8/7, veh/dex; KO N=8/8, veh/dex. **(I)** Mineralization quantification of calvaria-derived primary osteoblastic cell cultures from C57BL/6 mice treated with or without PF-431396 with veh or dex for 10 days stained using Alizarin Red S (405nm absorbance). veh, N=4/4, veh/dex; PF N=4/4, veh/dex, measured in triplicate. Bars represent means ± SD. **(A-G)** *$p<0.05$ vs corresponding placebo-treated mice and #$p<0.05$ vs placebo-treated WT mice by two-way ANOVA, Tukey post-hoc test. **(H-I)** *$p<0.05$ vs corresponding vehicle-treated cells and #$p<0.05$ vs vehicle-treated cells without GC by two-way ANOVA, Tukey post-hoc test.

Figure 4. Loss of Pyk2 signaling by genetic or pharmacologic means protects from GC-induced bone resorption by decreasing activity of individual osteoclasts and promoting osteoclast detachment from bone. (A-C and H) CTX, WT, N=7/7/7, placebo/GC1/GC2; KO N=7/6/6, placebo/GC1/GC2, TRAP5b, WT, N=7/6/6, placebo/GC1/GC2; KO N=7/6/6, placebo/GC1/GC2, CTX/TRAP5b, WT, N=7/5/6, placebo/GC1/GC2; KO N=7/6/6, placebo/GC1/GC2, were measured in blood collected 4 weeks after pellet implantation for WT or KO mice and CTX, veh, N=9/9, placebo/GC2; PF N=10/6, placebo/GC2, and TRAP5b, veh, N=9/9, placebo/GC2; PF N=10/6, placebo/GC2, were measured after 2 weeks for veh and PF-treated mice. **(D** and **I)** Osteoclast number (N.Oc/BS) and surface (Oc.S/BS) normalized to bone surface and marrow osteoclast number normalized to total marrow cavity area were determined in longitudinal sections of lumbar vertebra (L1-L3) for WT, N=6/6/6, placebo/GC1/GC2; KO N=6/6/6, placebo/GC1/GC2 mice, or of longitudinal distal femur sections, veh, N=6/8, placebo/GC2; PF N=8/5, placebo/GC2, for veh or PF-treated mice. **(E)** Expression of indicated genes in L4 bones is shown, WT, N=8/8/8, placebo/GC1/GC2; KO N=8/8/8, placebo/GC1/GC2. **(F)** Representative microscopy images of osteoclasts on cancellous bone surface or in the marrow of lumbar vertebra (L2) stained for TRAPase. Arrows point to osteoclasts fully attached to bone on top images from WT mice and osteoclasts partially attached on bottom images from KO mice. Scale bars: 25 μm. **(G)** Cartoons and representative high magnification images of WT and KO osteoclasts. Bars represent means ± SD. **(A-E)***$p<0.05$ vs corresponding placebo-treated mice and #$p<0.05$ vs placebo-treated WT mice, by two-way ANOVA, Tukey post-hoc test. **(H-I)**

*p<0.05 vs corresponding vehicle-treated mice and #p<0.05 vs placebo and vehicle-treated mice by two-way ANOVA, Tukey post-hoc test.

Figure 5. Decreased GC-induced resorption by genetic or pharmacologic inhibition of Pyk2 is due to osteoclast apoptosis, which overrides the prosurvival effects of GC on osteoclasts. **(A-B)** Apoptotic osteoclasts on bone (left graphs) and in the marrow (right graphs) were quantified in double stained TRAPase and TUNEL longitudinal sections of the distal femur. WT, N=6/6/6, placebo/GC1/GC2; KO N=6/6/6, placebo/GC1/GC2 or veh, N=5/6, placebo/GC2; PF N=6/6, placebo/GC2. Representative microscopy images of TUNEL negative osteoclasts fully attached to bone in WT mice and TUNEL positive osteoclasts partially attached to bone in KO mice are shown on the right of **(A)**. Scale bars: 20 μm. **(C-F)** Apoptosis of differentiated primary osteoclasts was quantified by evaluating loss of cell membrane integrity, nuclear condensation, and nuclear fragmentation. Osteoclasts derived from KO and WT mice (**C** and **D**) or from C57BL/6 mice treated with or without PF **(E** and **F)**, were treated *in vitro* with alendronate, dexamethasone (dex), or respective vehicles (veh), for 24 hours. TRAPase and hematoxylin staining were subsequently performed. Green star and arrow symbols indicate alive and apoptotic osteoclasts, respectively, in **D and F**. Scale bars: 20 μm. N=6. Bars represent means ± SD. **(A-B)** *p<0.05 vs corresponding placebo-treated mice and #p<0.05 vs placebo-treated mice, by two-way ANOVA, Tukey post-hoc test. **(C** and **E)** *p<0.05 vs corresponding vehicle-treated cells and #p<0.05 vs alendronate treated cells from WT or C57BL/6 mice by three-way ANOVA, Tukey post-hoc test.

Figure 6. Inhibition of the Pyk2/anoikis pathway represents a novel mechanistic approach to preserve skeletal integrity with GC excess. Activation of proline-rich tyrosine kinase 2 (Pyk2) is required for the opposing GC regulation of bone cell anoikis, depending on bone cell lineage, with anti-apoptotic effects for osteoclasts but pro-apoptotic effects for osteoblasts/osteocytes. Inhibiting Pyk2 activation prevents GC-induced bone loss and fragility by stimulating osteoclasts anoikis and preventing osteoblasts/osteocytes anoikis, without further suppressing bone renewal rate or altering biomechanical material properties. Targeting the Pyk2/anoikis pathway is a novel mechanistic approach to preserve skeletal integrity with GC, without undesirable skeletal complications.

Table 1. Genetic deletion of Pyk2 protects from GC-induced loss of bone strength

L6 axial compression (cancellous bone)	WT placebo	WT GC1	WT GC2	KO placebo	KO GC1	KO GC2
Structural (or extrinsic) mechanical properties						
Energy to Ultimate Force, mJ	4.1 ±0.8	*2.1 ±1.5	*2.0 ±1.4	#6.3 ±1.8	6.8 ±1.2	5.9 ±1.4
Ultimate Force, N	16.8 ±2.7	11.8 ±4.1	*9.5 ±3.3	#24.8 ±3.3	22.7 ±6.3	25.2 ±6.3
Stiffness, N/mm	71.7 ±14.9	83.0 ±19.4	61.0 ±23.1	#105.6 ±21.0	113.1 ±30.0	103.2 ±27.5
Material (or intrinsic) mechanical properties						
Toughness, mJ/mm^3	14.9 ±3.7	*9.1 ±4.7	*6.2 ±4.7	15.5 ±5.6	14.0 ±1.3	13.5 ±1.5
Ultimate Stress, MPa	1.8 ±0.4	1.3 ±0.3	1.4 ±0.5	1.8 ±0.3	1.6 ±0.6	1.7 ±0.4
Young's modulus, MPa	728.7 ±276.9	717.8 ±187.3	566.5 ±276.1	739.8 ±285.6	763.3 ±282.8	712.8 ±222.8

Biomechanical properties were measured in vertebral bone (L6) by axial compression testing. WT, N=10/10/9, placebo/GC1/GC2; KO N=10/9/7, placebo/GC1/GC2. *p<0.05 vs corresponding placebo-treated mice and #p<0.05 vs placebo-treated WT mice, by two-way ANOVA, Tukey post-hoc test.

Table 2. Pyk2 pharmacologic inhibition prevents from GC-induced bone fragility

3 point bending (cortical bone)	Veh placebo	Veh GC2	PF-431396 placebo	PF-431396 GC2

Structural (or extrinsic) mechanical properties				
Energy to Ultimate Force, mJ	2.9 ±0.4	*2.0 ±0.5	2.8 ±0.8	2.5 ±0.7
Ultimate Force, N	12.6 ±0.9	*10.9 ±0.6	12.5 ±1.4	11.7 ±1.9
Stiffness, N/mm	59.0 ±4.9	54.1 ±6.0	57.0 ±5.6	56.9 ±7.6
Material (or intrinsic) mechanical properties				
Toughness, mJ/mm^3	11.8 ±1.9	*8.4 ±1.7	11.4 ±1.5	11.6 ±1.4
Ultimate Stress, MPa	174.9 ±12.9	168.1 ±12.5	170.7 ±15.8	174.5 ±18.7
Young's modulus, MPa	2927.6 ±253.7	2892.7 ±397.5	2778.1 ±365.0	2966.2 ±112.5

Biomechanical properties were measured in the femoral mid-diaphysis by three-point bending; veh, N=9/9, placebo/GC2; PF N=10/6, placebo/GC2. *$p<0.05$ vs corresponding vehicle-treated mice and #$p<0.05$ vs placebo and vehicle-treated WT mice by two-way ANOVA, Tukey post-hoc test.

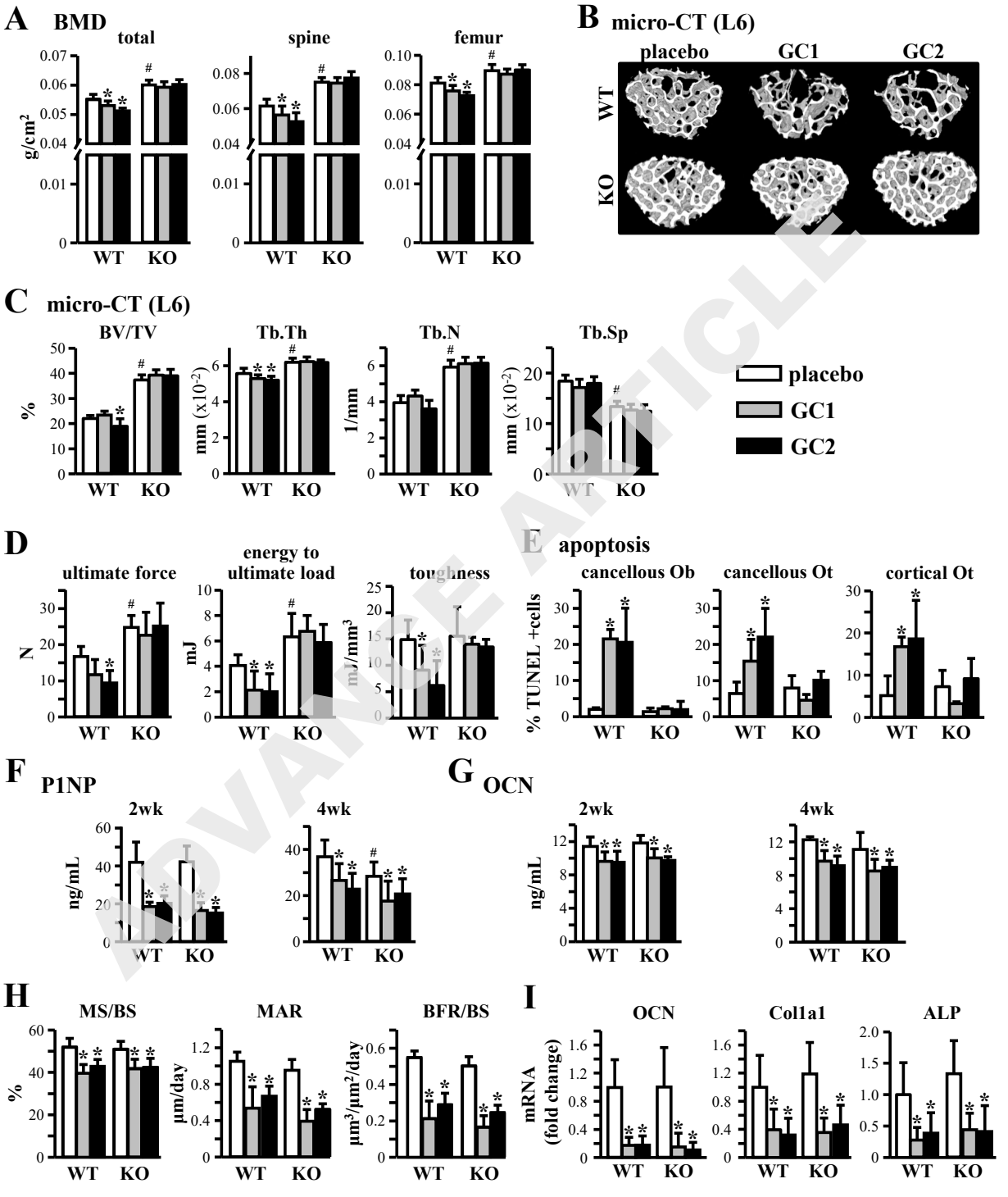

Figure 1

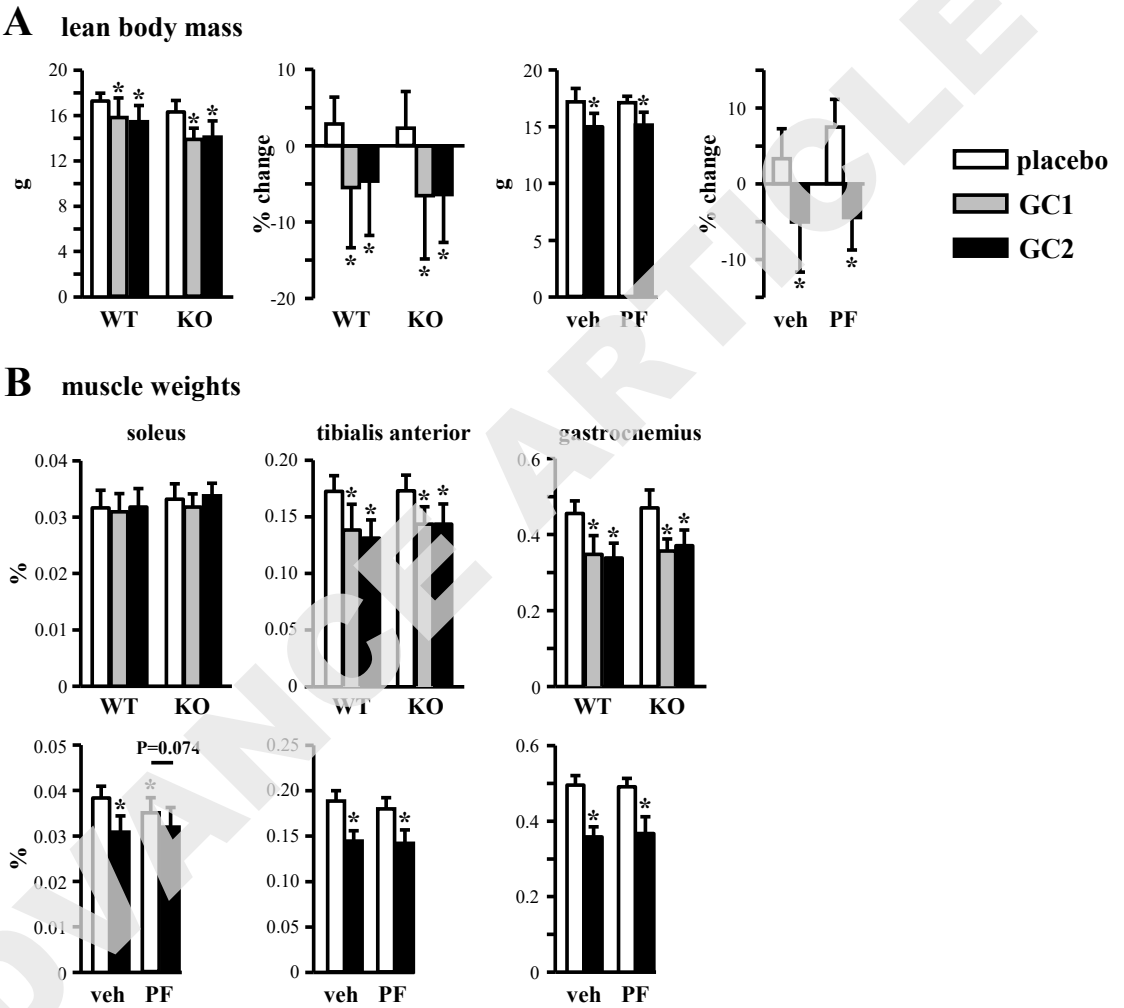

Figure 2

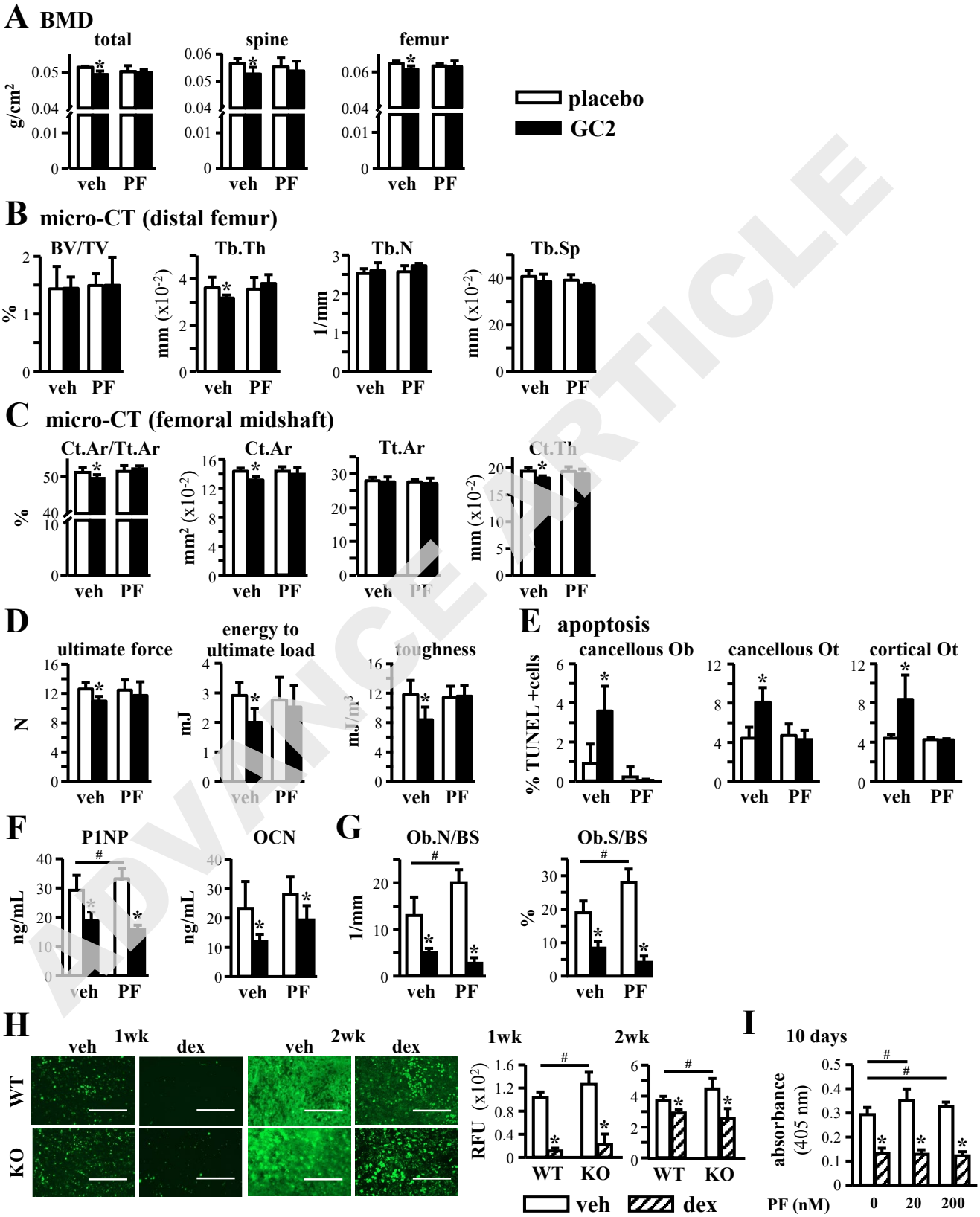

Figure 3

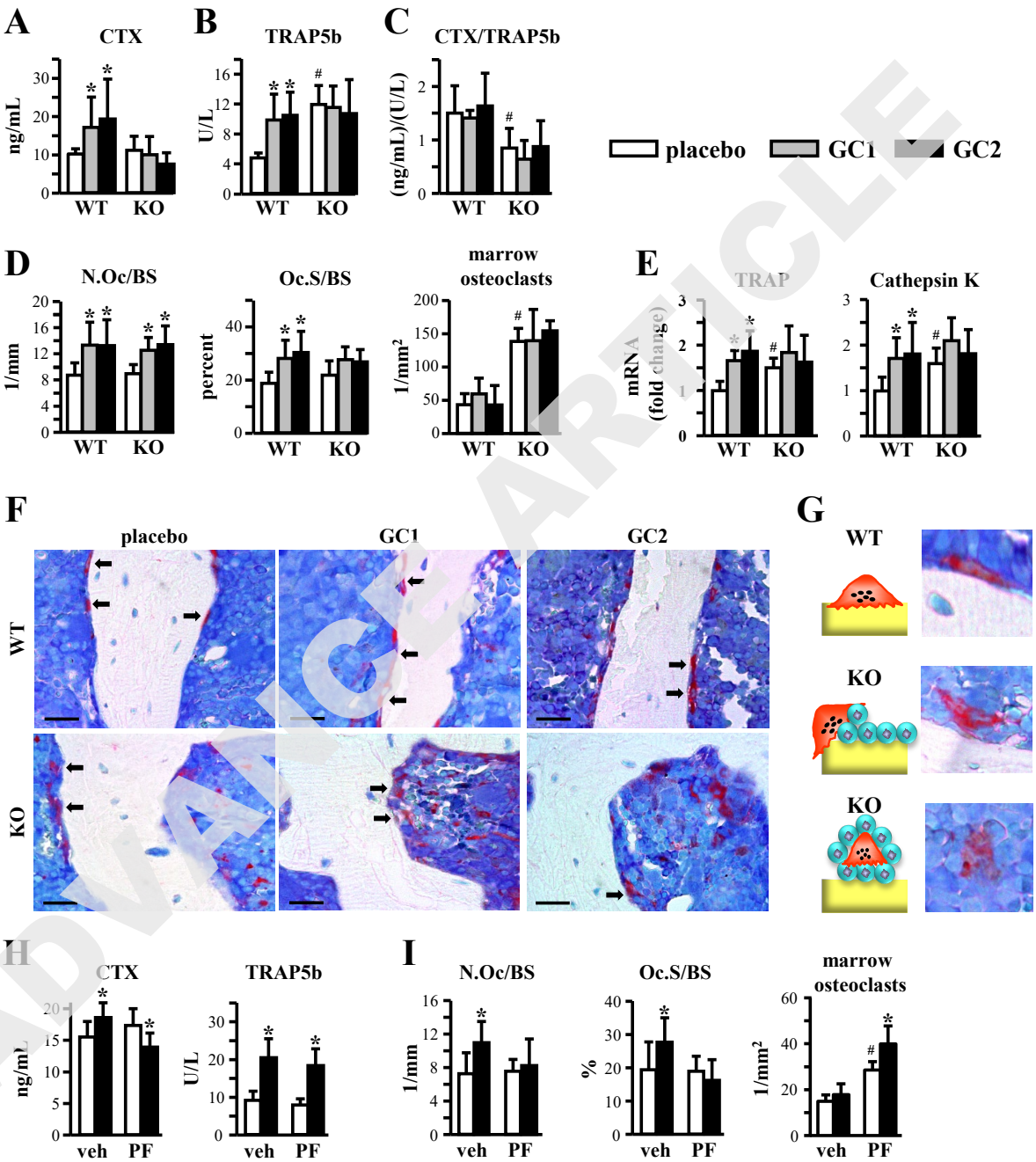

Figure 4

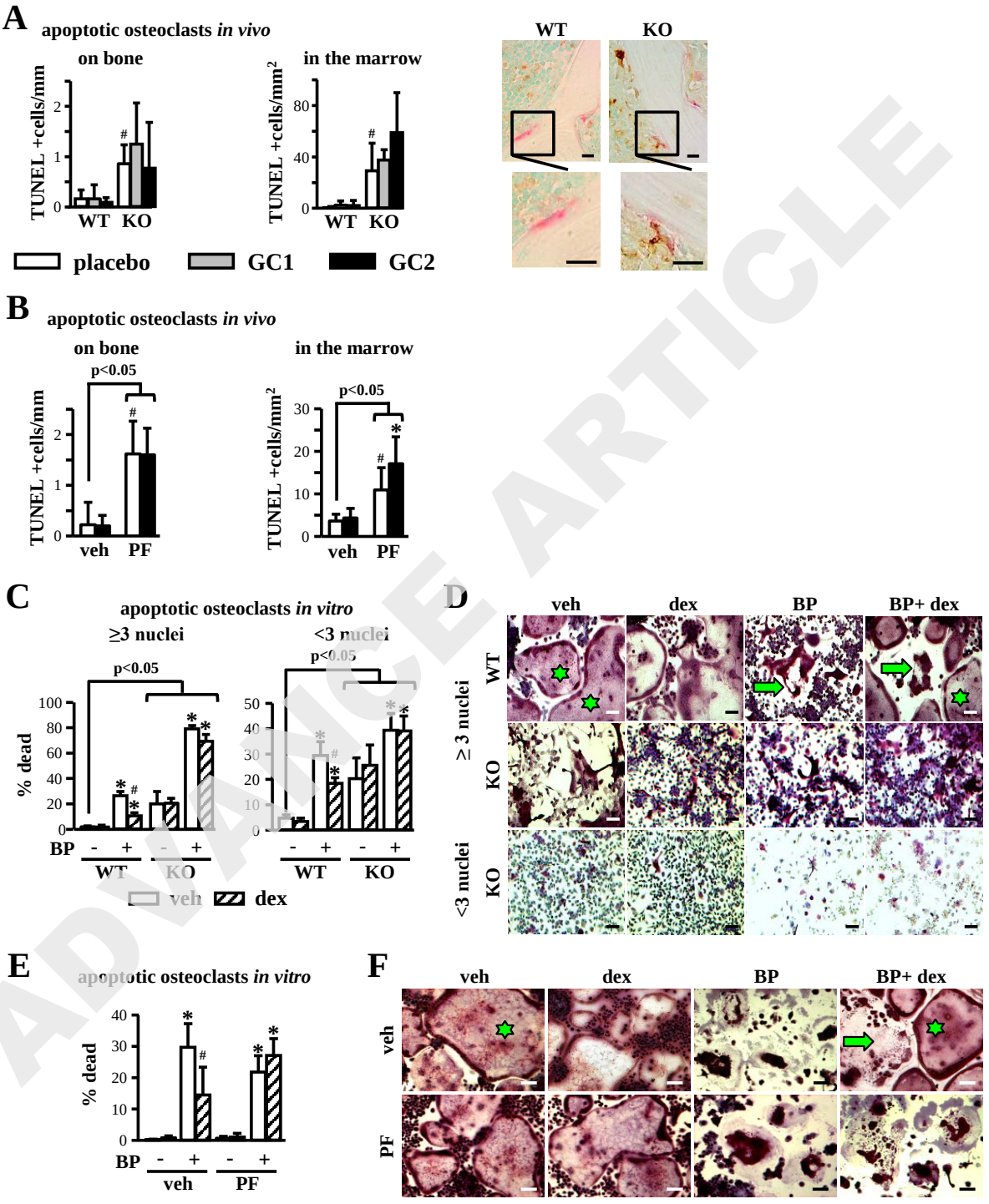

Figure 5

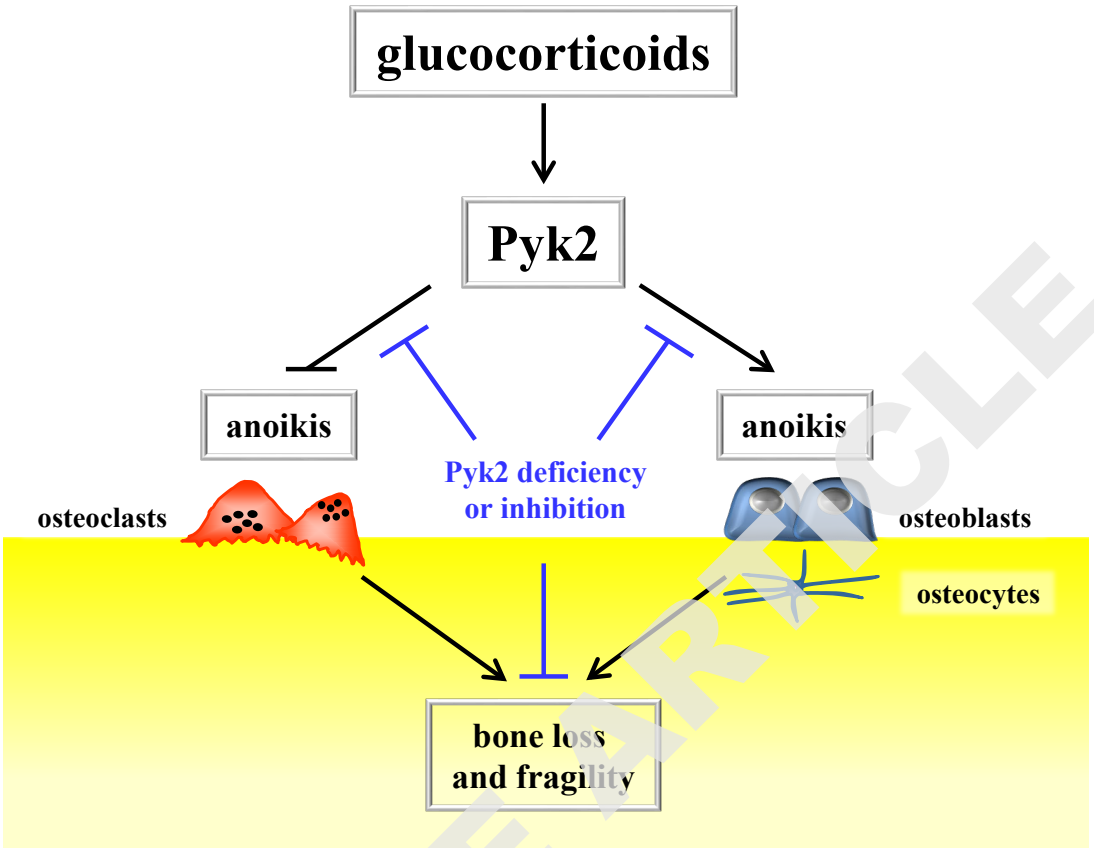

Figure 6